Relaxation processes of the light-induced giant injection magnetoresistance in semiconductor/granular-film heterostructures with cobalt nanoparticles

L. V. Lutsev,[1,*] L. A. Shelukhin,[1] A. I. Stognij,[2] and N. N. Novitskii[2]
[1]*Ioffe Physical-Technical Institute, 194021 St. Petersburg, Russia*
[2]*Scientific and Practical Materials Research Centre, National Academy of Sciences of Belarus, 220072 Minsk, Belarus*

(Received 29 January 2019; revised manuscript received 4 April 2019; published 23 April 2019)

We have studied relaxation processes of the photocurrent and the light-induced giant injection magnetoresistance ($IMR^{(ph)}$) in SiO_2(Co)/GaAs heterostructures, where the SiO_2(Co) structure is the granular SiO_2 film with Co nanoparticles, and have found that the photocurrent is accompanied by relaxation oscillations. Relaxation oscillations are caused by transitions between the photocurrent and electrons on the highest level in the interface quantum well. The light-induced magnetoresistance $IMR^{(ph)}$ reaches the maximum value in the avalanche onset region and has the local minimum at the higher voltage. It is found that the local minimum can been explained by delocalization of the highest level in the interface quantum well and by decrease of the probability of the backscattering process of injected electrons on deeper levels. SiO_2(Co)/GaAs heterostructures are proposed to use as efficient fast-response magnetic sensors operating without hysteresis at room temperature.

DOI: 10.1103/PhysRevB.99.134433

I. INTRODUCTION

Ferromagnet-semiconductor heterostructures are of great interest because of promising applications for spin-electronic devices and magnetic sensors [1–3]. Magnetic sensors have numerous applications in areas such as position sensing, speed detection, noncontact switching, vehicle detection, space exploration, electronic compasses, geophysical prospecting, nondestructive testing, biomedicine, and brain-function mapping [4–6].

The necessary condition for magnetic sensors is a high value of magnetoresistance. Extremely large magnetoresistance can be achieved in SiO_2(Co)/GaAs heterostructures, where the SiO_2(Co) is the SiO_2 film with Co nanoparticles [7–10]. Since the effect is expressed when electrons are injected from the granular film into the semiconductor, this magnetoresistance effect was named the giant injection magnetoresistance (IMR effect). For SiO_2(Co)/GaAs heterostructures with Co nanoparticles, the IMR value reaches 1000 (10^5%) at room temperature, which is two to three orders higher than the maximum values of the giant magnetoresistance (GMR) in metal magnetic multilayers [11–14] and the tunneling magnetoresistance (TMR) in magnetic tunnel junction structures [15–21]. High values of the IMR effect give us the opportunity to use the semiconductor/granular-film heterostructures as magnetic sensors with higher sensitivity.

High values of the IMR effect in SiO_2(Co)/GaAs heterostructures are explained by the theoretical model of a magnetic-field-controlled avalanche process provided by electrons passed through the spin-dependent potential barrier in the accumulation layer at the interface and by the spin-dependent current reduction caused by the backscattering process of injected electrons on exchange-split levels of the interface quantum well [9,10,22]. Besides the IMR effect, the interface region of SiO_2(Co)/GaAs heterostructures and the avalanche positive feedback are of great importance in the negative photoconductance and in the magnetic field enhancement of the photocurrent in the vicinity and above the GaAs band gap [23–25].

Although high values of the magnetoresistance in SiO_2(Co)/GaAs heterostructures have been obtained, relaxation processes accompanying the IMR effect have not been studied. This study can clarify the nature of transitions occurring in the interface region of SiO_2(Co)/GaAs heterostructures and is important for the production of fast-response magnetic sensors with higher sensitivity in comparison with GMR sensors [26,27].

In this paper, we study relaxation processes of the giant injection magnetoresistance in SiO_2(Co)/GaAs heterostructures induced by femtosecond light impulses. Sample preparation and characteristics of silicon-dioxide films with cobalt nanoparticles are presented in Sec. II. In Sec. III, we present the results of the IMR effect at direct current. Sharp growth of the magnetoresistance coefficient is observed in the avalanche onset region. Experimental results of the relaxation processes induced by femtosecond light impulses are considered in Sec. IV. Relaxation oscillations of the photocurrent and variations of the IMR value dependent on the applied voltage are observed. Experimental results are explained in Sec. V by a theoretical model based on variations of the density of electrons on exchange-split levels in the interface quantum well.

II. SAMPLE PREPARATION AND CHARACTERISTICS OF SILICON-DIOXIDE FILMS WITH COBALT NANOPARTICLES

The $(SiO_2)_{100-x}Co_x$ [SiO_2(Co)] films were prepared by the ion-beam deposition technique using a composite

*l_lutsev@mail.ru

TABLE I. Properties of SiO_2(Co) films sputtered on GaAs substrates.

No.	Film thickness (nm)	Co concentration x (at.%)
1	86	38
2	81	45
3	90	60
4	95	71
5	95	82

cobalt-quartz target onto GaAs substrates heated to 200 °C [9]. The Co concentration in the SiO_2 matrix was specified by a proportion of cobalt-quartz surface areas. *n*-GaAs substrates with thickness of 0.4 mm were of the (100)-orientation type. The substrate electrical resistivity was equal to 0.93×10^5 Ω cm. Prior to the deposition process, substrates were polished by a low-energy oxygen ion beam [28]. The roughness height of the polished surfaces was less than 0.5 nm.

The film composition was determined by the nuclear physical methods of element analysis [29]. The cobalt-to-silicon atomic ratio in the samples $(SiO_2)_{100-x}Co_x$/GaAs was measured by the Rutherford backscattering spectrometry of deuterons. For the samples studied, the relative content of cobalt x and the film thickness are listed in Table I. The average size of the Co particles was determined by the small-angle x-ray scattering and increased as the concentration of x grows: from 2.7 nm at $x = 38$ at.% to 4.4 nm at $x = 82$ at.%.

A protective Au layer with the thickness of 3–5 nm was deposited on the SiO_2(Co) films. The Au layer formed one ohmic contact in experiments, while the second contact was on the GaAs substrate. Electrical resistivity of SiO_2(Co) films was measured by the dc four-probe method on SiO_2(Co)/quartz heterostructures at room temperature. As the Co content increased, the resistivity of the SiO_2(Co) films decreased from 1.46×10^2 Ω cm (38 at.%) to 1.1 Ω cm (82 at.%). The film resistivity is much smaller than the resistivity of the GaAs. In this case, in experiments the applied voltage U primarily falls on the GaAs substrates.

It was found that SiO_2(Co) films sputtered on GaAs are inhomogeneous through the thickness. Small-angle x-ray scattering of synchrotron radiation in the grazing incidence geometry (GISAXS) and x-ray reflectivity showed a specific interface layer 70–75 Å thick separating bulk SiO_2(Co) granular film from the semiconductor substrate [30–32]. This layer was formed by a monolayer of flattened Co particles, which were laterally spaced apart much further than the particles in the bulk film. Using temperature-dependent polarized neutron reflectometry and magnetization measurements performed by a superconducting quantum interference device (SQUID), one found the occurrence of two types of magnetic nanoparticles with different blocking temperatures and magnetization.

The magnetic properties of SiO_2(Co) films have been studied by the ferromagnetic-resonance (FMR) spectra technique over frequency ranges of 37–41 GHz and 25–28 GHz at room temperature [33,34] and by the Brillouin light scattering (BLS) method [35–37]. A sharp increase in the FMR linewidth ΔH with a decreasing concentration of cobalt nanoparticles was found [33]. The effect of considerable FMR linewidth broadening has been accounted for by the spin-polarized relaxation mechanism [38]. The anomalous local fall in the dependence of the magnetization of SiO_2(Co) films on the Co concentration of granular nanostructures has been detected in the range of 50–60 at.% Co [34]. The observed peculiarity of the magnetization dependence has been explained by the influence of the semiconductor substrate on the spin polarization of Co particles in the granular film.

The BLS method gives the possibility to study dipole-exchange spin waves propagated in SiO_2(Co) films [35–37]. The BLS measurements were carried out in the Damon-Eshbach geometry. The saturating magnetic field H was applied parallel to the plane of the film and the direction of propagation of the spin waves was normal to H. Since spin waves are very sensitive to the inhomogeneity of magnetic parameters, spin disorder, and conductivity of an object near or inside which these waves propagate, they can be used to determine magnetic and electrical characteristics of the objects under investigation. The analysis of dispersion curves obtained in [35–37] has been used to determine parameters of heterostructures consisting of a SiO_2 film with Co nanoparticles on a GaAs substrate [39]. It has been found from the shape of dispersion curves of the surface spin waves that in the film near the interface, spins of the Co nanoparticles are close to a ferromagnetic ordering, whereas near the free surface, the spin orientation of nanoparticles is more chaotic. It has been revealed that a conducting layer is formed in GaAs, and the SiO_2(Co) film near the interface has an increased conductivity.

The field dependencies of magnetization have been measured at 300 K with the applied magnetic field parallel and perpendicular to the SiO_2(Co) films [35]. It was found that films are fully saturated for an applied field of 2000 Oe for the parallel orientation. With the field perpendicular to the film, the value of 9000 Oe is necessary to reach the saturation.

III. IMR EFFECT AT DIRECT CURRENT

We have studied current-voltage characteristics and magnetoresistance in SiO_2(Co)/GaAs heterostructures (Table I) at direct current. One contact was on the semiconductor substrate, and the other was on the SiO_2(Co) granular film. The first contact was prepared by a silver paste on the GaAs back surface. Figure 1(a) illustrates the effect of the magnetic field on the current-voltage characteristic at room temperature in the case of the electron injection into the GaAs substrate for the SiO_2(Co)/GaAs structure (sample no. 4) with 71 at.% Co. For $U > 55$ V, a sharp increase in the current due to the process of impact ionization is observed. The applied magnetic field postpones this process to higher electric fields. The magnetic field H is parallel to the film surface.

One can observe that the current density j decreases with growth of the magnetic field H [Fig. 1(b)]. The further magnetic field lowering increases the current, but the descending and ascending current branches do not coincide with forming a hysteresis. The hysteresis is caused by the avalanche process developed in the GaAs. At the growth of the magnetic field, the quenching of the avalanche occurs at higher field values than the onset of the avalanche at magnetic field lowering. If the avalanche process is stable (for example, for the voltage

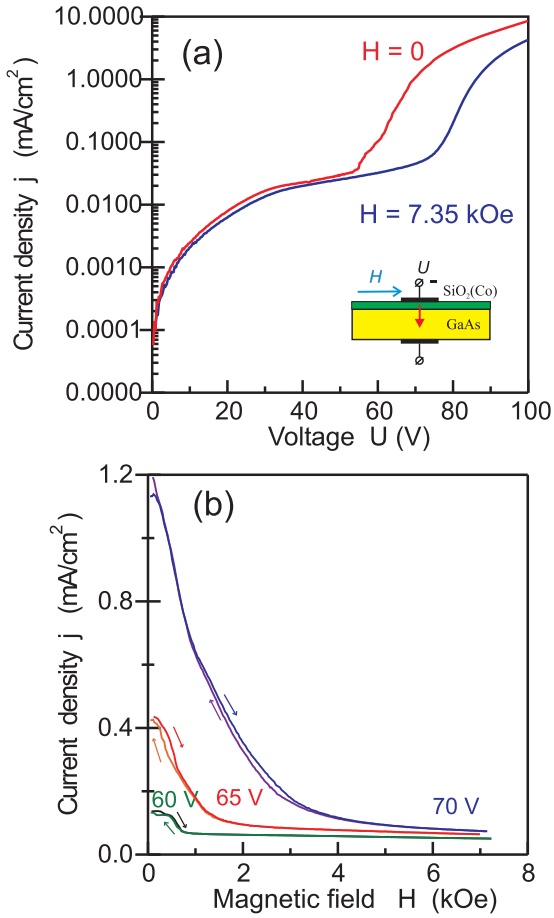

FIG. 1. (a) Current-voltage characteristic for the electron injection into the semiconductor for the SiO_2(Co)/GaAs structure with 71 at.% Co (sample no. 4) at the magnetic field $H = 7.35$ kOe and without a magnetic field. (b) Current density j flowing in the sample no. 4 at the voltage $U = 60$, 65, and 70 V vs the magnetic field H at field growth and at decrease of the magnetic field, respectively. H is parallel to the surface of the SiO_2(Co) film.

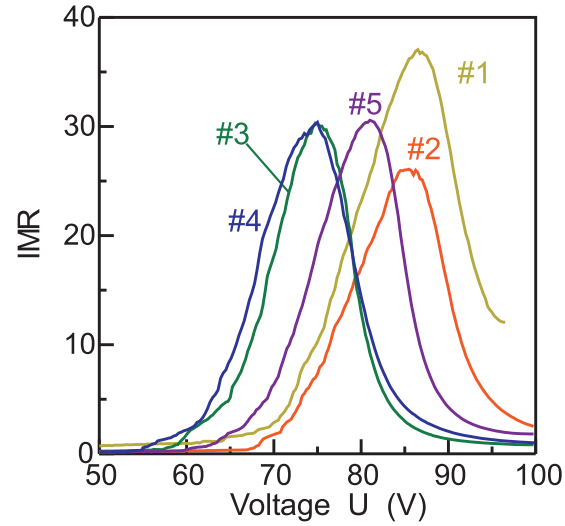

FIG. 2. The injection magnetoresistance IMR vs the applied voltage U at room temperature for the SiO_2(Co)/GaAs structures at the magnetic field $H = 7.35$ kOe. H is parallel to the surface of the SiO_2(Co) film.

70 V in the range 150–1000 Oe), then there is no hysteresis and the branches coincide.

The injection magnetoresistance coefficient IMR is defined by the ratio [7–10]

$$\mathrm{IMR} = \frac{R(H) - R(0)}{R(0)} = \frac{j(0) - j(H)}{j(H)}, \qquad (1)$$

where $R(0)$ and $R(H)$ are the resistances of the SiO_2(Co)/GaAs heterostructure without a field and in the magnetic field H, respectively; $j(0)$ and $j(H)$ are the current densities flowing in the heterostructure in the absence of a magnetic field and in the field H. The IMR ratio for the SiO_2(Co)/GaAs heterostructures (Table I) versus the applied voltage U at room temperature at the magnetic field $H = 7.35$ kOe is shown in Fig. 2. The magnetic field H is parallel to the film. As seen from Fig. 1, the applied magnetic field suppresses the avalanche process and the current flowing in the heterostructure decreases. As a result, the suppression of the avalanche process causes a sharp growth of the magnetoresistance coefficient in the avalanche onset region, where the magnetoresistance reaches highest values (Fig. 2). The location of the IMR coefficient maximum depends on the Co content x. For samples no. 3 and no. 4 with 60 at.% Co and 71 at.% Co, respectively, the IMR maximum is observed at the voltage $U = 75$ V. For higher (sample no. 5 with 82 at.% Co) and lower (samples no. 1 with 38 at.% Co and no. 2 with 45 at.% Co) cobalt concentrations, the voltage at which the magnetoresistance reaches maximum is shifted to higher values.

According to [7], the IMR effect is observed at any orientation of the magnetic field. But, due to the demagnetization factor of the film, the highest value of the IMR coefficient is reached at a magnetic field parallel to the film surface.

The above-mentioned study of current-voltage characteristics and magnetoresistance in SiO_2(Co)/GaAs heterostructures performed at direct current shows that the IMR dependencies are similar for samples with different cobalt concentrations. The only difference is in the location of the IMR coefficient maximum. Taking this into account, in order to study relaxation processes induced by femtosecond light impulses, we have chosen the SiO_2(Co 60 at.%)/GaAs heterostructure (sample no. 3).

IV. RELAXATION PROCESSES INDUCED BY FEMTOSECOND LIGHT IMPULSES

To study the injection magnetoresistance IMR and relaxation processes induced by femtosecond impulses, we used the setup presented in Fig. 3. According to the theoretical model developed in [9,10,22], due to the exchange interaction between electrons in the interface quantum well in the semiconductor and d electrons of Co, the quantum well in GaAs contains exchange-split levels partially filled by electrons. Therefore, one can expect an appearance of spin-dependent effects. For this purpose, in order to detect possible spin-dependent effects, we used circularly polarized light in Faraday's geometry in which the magnetic field was normal to the SiO_2(Co) film surface. The duration of the light impulses

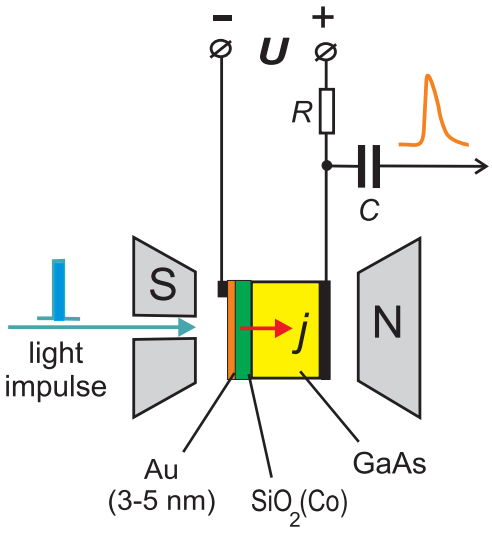

FIG. 3. Block diagram of the setup used for the study of the injection magnetoresistance IMR and relaxation processes induced by femtosecond light impulses.

was equal to 180 fs and the pulse repetition was of 5 kHz. In experiment, we used the light beam with helicities of two signs: the helicity vector has been chosen parallel and antiparallel to the orientation of the magnetic field. The light fluence was equal to 5 mJ/cm^2. The light beam has been passing through the Au contact layer, the SiO_2(Co) film, and the GaAs substrate.

The current flowing in the SiO_2(Co)/GaAs structure was the sum of the direct current j_0 and the photocurrent $j(t)$. The photocurrent dependencies were obtained for photon energies $E = 1.35$ and 1.4 eV. The GaAs band-gap energy $E_g = \sim 1.4$ eV was determined as a maximum of the derivative of the optical density [23]. The highest growth of the photocurrent exists in the narrow range of photon energies of 1.38–1.41 eV near the band-gap energy E_g of the GaAs. Relaxation processes induced by femtosecond impulses of light were detected by a microwave frequency band oscillograph. Parameters of the low-pass RC filter have been chosen such that $RC > 10$ ms.

The relaxation process of the current flowing in the SiO_2(Co 60 at.%)/GaAs heterostructure (sample no. 3) induced by light impulse at different applied voltages in the magnetic field $H = 12$ kOe and without a magnetic field at the photon energy 1.35 eV is shown in Fig. 4. In the start region of the relaxation process, relaxation oscillations are observed. After the light impulse, at the time t_2, the photoinduced current reaches its maximum value j_2. At the time $t > t_2$, the photoinduced current exponentially decreases. One can observe that the magnetic field suppresses the current. The current suppression reaches its maximum at $t = t_2$.

Figure 5 presents amplitude j_1 of the current peak in the start region of the relaxation process and the maximum of the photoinduced current j_2 flowing in the SiO_2(Co 60 at.%)/GaAs heterostructure (sample no. 3) versus the applied voltage U at photon energies $E = 1.35$ and 1.4 eV in the magnetic field $H = 12$ kOe. Within the experimental error, the photoinduced currents do not depend on the sign of

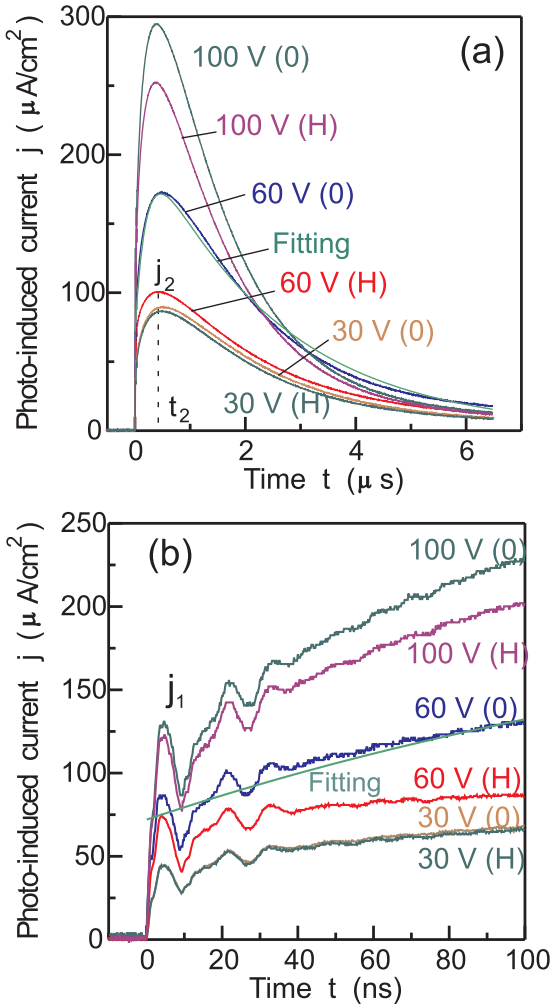

FIG. 4. Relaxation process of the current flowing in the SiO_2(Co 60 at.%)/GaAs heterostructure (sample no. 3) induced by light impulse at different applied voltages in the magnetic field $H = 12$ kOe [curves 30 $V(H)$, 60 $V(H)$, 100 $V(H)$] and without a magnetic field [curves 30 $V(0)$, 60 $V(0)$, 100 $V(0)$] at the photon energy 1.35 eV. (a) Large timescale; (b) start region of the relaxation process. The curve fitting is presented for the 60 $V(0)$ dependence.

the light helicity. One can see that at $E = 1.4$ eV, the current-voltage dependencies have maximum points. For the current j_1, this maximum point is observed at $U = 80$ V, and for the current j_2, the maximum is located at $U = 90$ V, respectively. In contrast with this, at $E = 1.35$ eV the current-voltage dependencies have no maximum points. The photoinduced currents j_1 and j_2 increase with growth of the voltage.

At the time t_2, the photoinduced current reaches its maximum value j_2. Figure 6 presents the time t_2 versus the applied voltage U for the SiO_2(Co 60 at.%)/GaAs heterostructure (sample no. 3) at photon energies $E = 1.35$ and 1.4 eV in the magnetic field $H = 12$ kOe. One can see that the time t_2 decreases with growth of the voltage U. Similar to dependencies in Fig. 5, within the experimental error the time t_2 does not depend on the sign of the light helicity.

The photoinduced current j_2 flowing in the SiO_2(Co 60 at.%)/GaAs heterostructure at the time t_2 increases with increase of the applied voltage U. As we can see from Fig. 7(a)

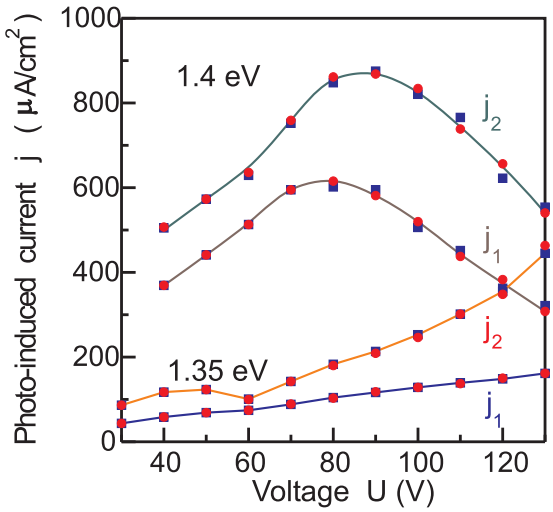

FIG. 5. Amplitude j_1 of the current peak in the start region of the relaxation process and the maximum of the photoinduced current j_2 flowing in the SiO_2(Co 60 at.%)/GaAs heterostructure (sample no. 3) vs the applied voltage U at photon energies 1.35 and 1.4 eV in the magnetic field $H = 12$ kOe. Squares (■) and circles (●) are experimental points obtained at different signs of the light helicity: the helicity vector is parallel and antiparallel to the orientation of the magnetic field, respectively.

(sample no. 3), the photoinduced current is suppressed by the magnetic field.

It should be noted that the injection magnetoresistance coefficient $\mathrm{IMR}^{(ph)}$ [Fig. 7(b)], which is calculated in accordance with relation (1),

$$\mathrm{IMR}^{(ph)} = \frac{j_2(0) - j_2(H)}{j_2(H)},$$

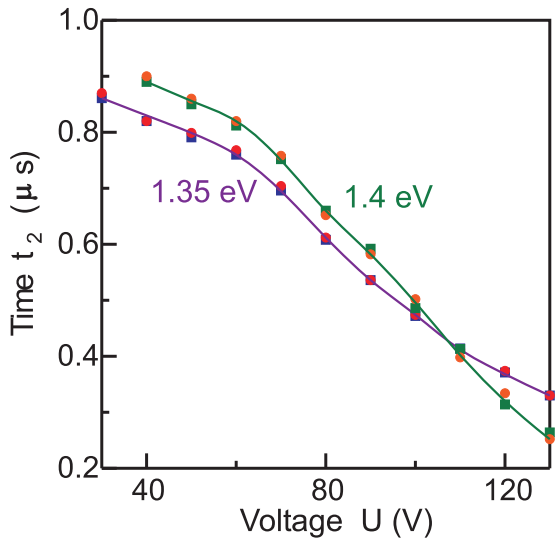

FIG. 6. Time t_2 of appearance of the maximum photoinduced current flowing in the SiO_2(Co 60 at.%)/GaAs heterostructure (sample no. 3) vs the applied voltage U at photon energies 1.35 and 1.4 eV in the magnetic field $H = 12$ kOe. Squares (■) and circles (●) are experimental points obtained at different signs of the light helicity: the helicity vector is parallel and antiparallel to the orientation of the magnetic field, respectively.

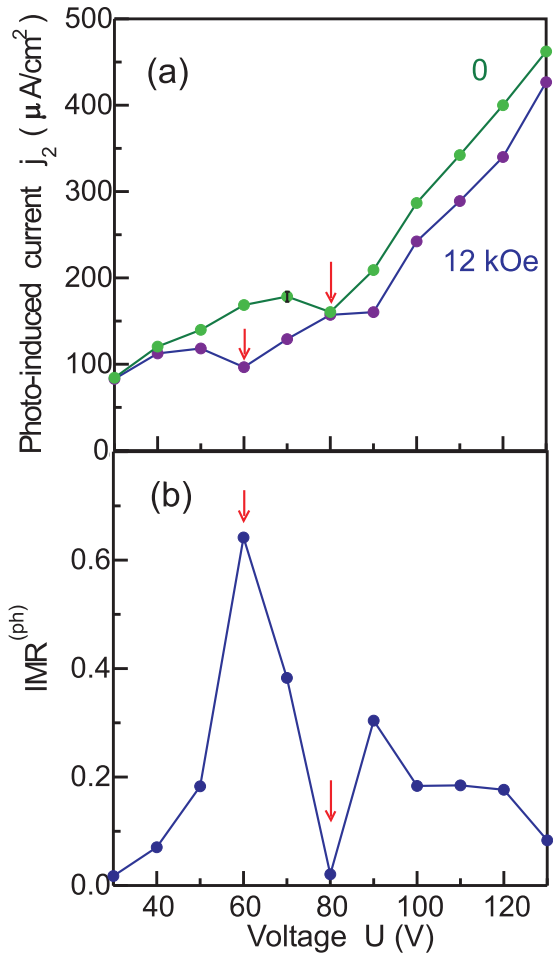

FIG. 7. (a) Maximum of the photoinduced current j_2 flowing in the SiO_2(Co 60 at.%)/GaAs heterostructure (sample no. 3) vs the applied voltage U in the magnetic field $H = 12$ kOe and without a magnetic field at the photon energy 1.35 eV. (b) The injection magnetoresistance $\mathrm{IMR}^{(ph)}$ vs the applied voltage U measured at the time t_2. The error estimation is presented for the photoinduced current at the applied voltage $U = 70$ V in the zero magnetic field.

reaches the maximum value in the avalanche onset region ($U = 60$ V) and is equal to zero at the voltage $U = 80$ V. This feature of the $\mathrm{IMR}^{(ph)}$ dependence is caused by delocalization of the highest level in the interface quantum well and by decrease of the probability of the backscattering process of injected electrons on deeper levels. This phenomenon is considered in the next section.

V. DISCUSSION

Explanation of the experiment is based on the theoretical model developed in [9,10,22]. In SiO_2(Co)/GaAs heterostructures, the difference of chemical potentials between the SiO_2(Co) film and the GaAs determines bending of the semiconductor conduction band (Fig. 8) and forms a quantum well (accumulation electron layer) in the semiconductor near the interface. Due to the exchange interaction between electrons in the quantum well in the semiconductor and d electrons of Co, the quantum well contains exchange-split levels.

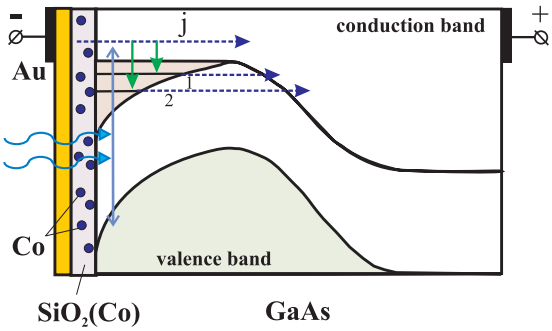

FIG. 8. Electronic energy band structure and exchange-split levels in the quantum well at the interface region in the granular-film SiO_2(Co)/GaAs heterostructure. 1 and 2 mark exchange-split levels.

High values of the magnetoresistance effect in SiO_2(Co)/GaAs heterostructures have been explained by magnetic-field-controlled onset of the impact ionization and by the electron accumulation in the quantum well in the semiconductor interface region induced by the backscattering process of injected electrons on exchange-split levels. The spin-dependent potential barrier is formed in the accumulation electron layer in the semiconductor near the interface. The potential barrier is due to the exchange interaction between electrons in the accumulation electron layer in the GaAs and d electrons of Co. The impact ionization induced by injected electrons produces holes, which move and are accumulated in the region of the potential barrier. Due to the formed hole positive feedback, small variations in the barrier height give great changes in the current. The applied magnetic field increases the height and reduces the transparency of the barrier. This suppresses the onset of the impact ionization and changes the potential distribution. The model developed in [9,10,22] can explain some features of the experimental results. Specifically, the existence of localized electron states in the accumulation layer results in high values of the barrier in the SiO_2(Co)/GaAs. This leads to the temperature-peak-type character of the IMR observed in [9]. Maxima of IMR peaks correspond to one exchange-split level in the accumulation layer.

In order to explain the relaxation processes of the photocurrent, we consider the action of the light impulse on the SiO_2(Co)/GaAs heterostructure (Fig. 8). The voltage U is applied on the heterostructure contacts and, consequently, the current flows through the heterostructure. We consider a small contact area and, after this, generalize results on the heterostructure contact. The light impulse generates additional electrons in the conduction band and induces a photocurrent. The dynamics of the photocurrent caused by these additional electrons and variations of densities of electrons on exchange-split levels 1 and 2 can be determined by the equation

$$\frac{\partial \vec{n}}{\partial t} = \mathcal{D}\vec{n} + \vec{f}(t), \tag{2}$$

where

$$\vec{n} = \begin{pmatrix} n_j \\ n_1 \\ n_2 \end{pmatrix}.$$

Here, n_j is the density of electrons induced by light. The photocurrent is determined by n_j, $j = en_j v$, where e is the electron charge and v is the electron velocity. n_1 is the variation of the density of electrons on level 1 (first level) in comparison with the thermodynamic equilibrium density. By analogy, n_2 is the variation of the density of electrons on level 2 (second level). The matrix $\mathcal{D}$ is

$$\mathcal{D} = \begin{pmatrix} d_{00} & d_{01} & d_{02} \\ d_{10} & d_{11} & d_{12} \\ d_{20} & d_{21} & d_{22} \end{pmatrix} = \begin{pmatrix} -(a_1+a_2) & (b_1 - V_1) & (b_2 - V_2) \\ a_1 & -(c+b_1) & 0 \\ a_2 & c & -b_2 \end{pmatrix}, \tag{3}$$

where a_1 and a_2 are the probabilities of transitions of photocurrent electrons on the first and second levels per unit of time, respectively. V_1 and V_2 determine the Coulomb influence of electrons localized on the first and second levels, respectively, on the photocurrent j. The increase of electrons on the levels leads to a decrease of the current j. b_1 and b_2 are the probabilities of electron tunneling per unit of time through the barrier from levels 1 and 2, respectively. c is the probability of the electron transition per unit of time from the first level on the second level.

The term $\vec{f}(t)$ denotes the generation of the photocurrent by the light. Taking into account that the impulse width of light is, to a great extent, less than the observed relaxation times, one can write the term $\vec{f}(t)$ as

$$\vec{f}(t) = \begin{pmatrix} A\delta(t) \\ 0 \\ 0 \end{pmatrix},$$

where A is the coefficient.

After the action of the light impulse, the solution of Eq. (2) can be written in the form [40]

$$\vec{n}(t) = \sum_{k=1}^{n} C^{(k)} \vec{\xi}^{(k)} \exp(\lambda^{(k)} t), \tag{4}$$

where the eigenvalues $\lambda^{(k)}$ are determined by the equation

$$\begin{aligned} &\det(\mathcal{D} - \lambda^{(k)}\mathcal{I}) \\ &= (d_{00} - \lambda^{(k)})(d_{11} - \lambda^{(k)})(d_{22} - \lambda^{(k)}) - d_{12}d_{21}(d_{00} - \lambda^{(k)}) \\ &\quad - d_{02}d_{20}(d_{11} - \lambda^{(k)}) - d_{10}d_{01}(d_{22} - \lambda^{(k)}) \\ &\quad + d_{01}d_{12}d_{20} + d_{02}d_{21}d_{10} = 0, \end{aligned} \tag{5}$$

where $\mathcal{I}$ is the identity matrix. The eigenvectors $\vec{\xi}^{(k)}$ are found from the equation

$$(\mathcal{D} - \lambda^{(k)}\mathcal{I})\vec{\xi}^{(k)} = 0.$$

In the experiment, we observe relaxation oscillations; consequently, one of the eigenvalues must be complex ($\lambda^{(1)} = \mathrm{Re}\lambda^{(1)} + i\mathrm{Im}\lambda^{(1)}$, $\mathrm{Re}\lambda^{(1)} \neq 0$, and $\mathrm{Im}\lambda^{(1)} \neq 0$). The second eigenvalue $\lambda^{(2)}$ is real. Since the probability b_1 of electron tunneling from the first level is, to a great extent, higher

than the probability b_2 of electron tunneling from the deeper second level, and taking into account that the probabilities of transitions on the deeper second level are smaller than the probabilities of transitions on the higher first level ($c < b_1$, $a_2 < a_1$), from Eq. (5) one can approximately calculate the relaxation time τ_1 and the circular frequency of relaxation oscillations,

$$\tau_1 = \frac{-1}{\mathrm{Re}\lambda^{(1)}} = \frac{2}{a_1 + b_1},$$
$$\omega = \mathrm{Im}\lambda^{(1)} = \frac{1}{2}[4a_1V_1 - (a_1 + b_1)^2]^{1/2}. \quad (6)$$

In this case, we take into account only the interaction between the photocurrent and the variation of the electron density n_1. The influence of the second level on the photocurrent j and, consequently, the term $(b_2 - V_2)$ in the $\mathcal{D}$ matrix (3) is ignored. Relaxation oscillations are observed if the Coulomb term satisfies the inequality

$$V_1 > \frac{1}{4a_1}(a_1 + b_1)^2.$$

In our experimental study, we observe relaxation oscillations (6) with the frequency of $\omega/2\pi = 100$ MHz. Within the experimental error, the relaxation oscillation frequency $\omega/2\pi$ is not varied under the magnetic field action and with increase of the applied voltage U.

In contrast with the relaxation time τ_1, which can be found by relation (6), in order to find the eigenvalue $\lambda^{(2)}$ and the relaxation time τ_2, it is necessary to solve the cubic equation (5) without any approximations.

Taking into account the form of the relaxation solution (4) and the complex-valued form of the eigenvalue $\lambda^{(1)}$, we can find the relaxation of the photocurrent $j(t)$ as

$$j(t) = -\frac{B_1}{2}\exp(\lambda^{(1)}t) - \frac{B_1}{2}\exp(\lambda^{(1)*}t) + B_2\exp(\lambda^{(2)}t)$$
$$= -B_1\exp\left(\frac{-t}{\tau_1}\right)\cos(\omega t) + B_2\exp\left(\frac{-t}{\tau_2}\right), \quad (7)$$

where $\lambda^{(1)} = -1/\tau_1 + i\omega$ and $\lambda^{(2)} = -1/\tau_2$. B_1 and B_2 are coefficients connected with the current j_1 (Fig. 4) by relation $j_1 = B_2 - B_1$.

The above-mentioned consideration has been done for small contacts and interface areas. Relaxation times τ_1, τ_2 and the oscillation frequency $\omega/2\pi$ in relation (7) may be different at different interface points. Integrating the current $j(t)$ (7) over the interface surface S, we find the current flowing in the heterostructure,

$$\bar{j}(t) = -B_1E_1(t) + B_2E_2(t), \quad (8)$$

where

$$E_1(t) = \int_S \exp\left(\frac{-t}{\tau_1}\right)\cos(\omega t)\rho_1(\tau_1,\omega)\,d\tau_1 d\omega,$$
$$E_2(t) = \int_S \exp\left(\frac{-t}{\tau_2}\right)\rho_2(\tau_2)\,d\tau_2,$$

and $\rho_1(\tau_1,\omega)$, $\rho_2(\tau_2)$ are distributions. Integrations are performed over the interface surface S. Deviation of the distribution $\rho_1(\tau_1,\omega)$ from the homogeneous distribution $\delta(\tau_1 - \tau_1^{(0)})\delta(\omega - \omega^{(0)})$, where $\tau_1^{(0)}$ and $\omega^{(0)}$ are average values of the relaxation time τ_1 and the relaxation oscillation ω, respectively, results in decrease of the relaxation oscillation amplitude.

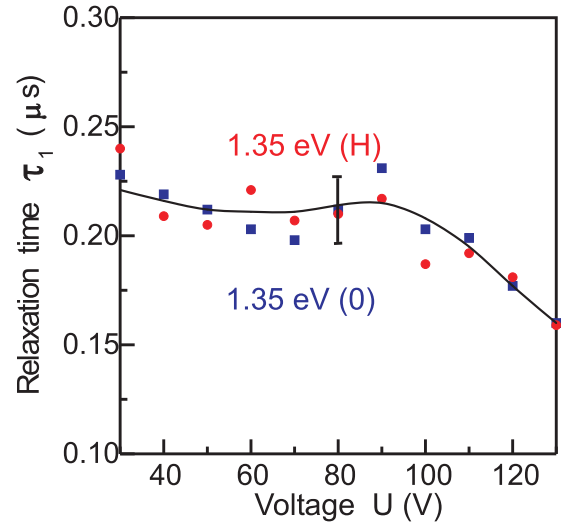

FIG. 9. Relaxation time τ_1 of the photoinduced current flowing in the SiO_2(Co 60 at.%)/GaAs heterostructure (sample no. 3) in the magnetic field $H = 12$ kOe [•: curve 1.35 eV(H)] and without a magnetic field [■: curve 1.35 eV(0)] at the photon energy 1.35 eV.

The maximum of the photoinduced current j_2 at $t = t_2$ in Fig. 4(a) can be determined as the zero derivative of the current $\bar{j}(t)$ (8) with respect to the time t,

$$\frac{\partial\bar{j}(t)}{\partial t} = 0.$$

In order to find the relaxation times τ_1 and τ_2, we have fitted experimental relaxation curves of the photocurrent by the theoretical dependence $\bar{j}(t)$ given by relation (8) with distributions,

$$\rho_1(\tau_1,\omega) = \mu(\omega)\delta\left(\tau_1 - \tau_1^{(0)}\right),$$
$$\rho_2(\tau_2) = \delta\left(\tau_2 - \tau_2^{(0)}\right),$$
$$\bar{j}(t) = -\bar{B}_1\exp\left(\frac{-t}{\tau_1}\right) + B_2\exp\left(\frac{-t}{\tau_2}\right). \quad (9)$$

The coefficient $\bar{B}_1$ in relation (9) is the constant obtained by time averaging of the relaxation oscillations,

$$\bar{B}_1 = B_1\left\langle\int_S \cos(\omega t)\mu(\omega)\,d\omega\right\rangle_t.$$

In this case, we ignore oscillations. The curve fitting is shown in Fig. 4 for the 60 $V(0)$ dependence. The relaxation time τ_1 of the photoinduced current flowing in the SiO_2(Co 60 at.%)/GaAs heterostructure in the magnetic field $H = 12$ kOe and without a magnetic field at the photon energy 1.35 eV is presented in Fig. 9. One can see that within the experimental error, the relaxation time τ_1 does not depend on the magnetic field. At high values of the applied voltage $U >$ 90 V, the small decrease of the relaxation time τ_1 is observed. According to relation (6), the relaxation time τ_1 is determined

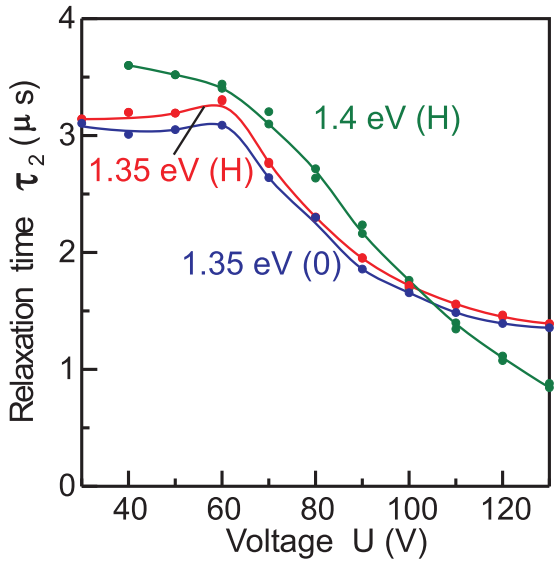

FIG. 10. Relaxation time τ_2 of the photoinduced current flowing in the SiO_2(Co 60 at.%)/GaAs heterostructure (sample no. 3) in the magnetic field $H = 12$ kOe [curves 1.35 eV(H) and 1.4 eV(H)] and without a magnetic field [curve 1.35 eV(0)] at photon energies 1.35 and 1.4 eV.

by transitions and influence between the photocurrent and electrons on the first level.

Dependencies of the relaxation time τ_2 of the photoinduced current flowing in the same heterostructure in the magnetic field $H = 12$ kOe and without a magnetic field at photon energies 1.35 and 1.4 eV versus the voltage U are presented in Fig. 10. It should be noted that the voltage growth results in a significant decrease of the relaxation time τ_2. In addition, in the magnetic field, the relaxation time τ_2 increases. In contrast with the relaxation time τ_1, high values of the time τ_2 are caused by electron transitions occurring on the deeper second level.

The above-mentioned model of the dynamics of the photocurrent with exchange-split levels in the interface quantum well [Eq. (2)] can explain the zero value of the injection magnetoresistance coefficient [Fig. 7(b)] at the voltage $U =$ 80 V. Indeed, voltage growing bends the semiconductor conduction band. As a result of the bending, the higher first level (Fig. 8) can be delocalized. In this case, the first level drops out from the photocurrent dynamics model and, besides the second level, it is necessary to take into consideration deeper levels in the quantum well. The probability of the backscattering process of injected electrons on deep levels is small [10]. This leads to small variations of the density of electrons on these levels, and, therefore, to low values of the magnetoresistance $IMR^{(ph)}$. The further growth of the voltage results in increase of bending of the conduction band and the subsequent level lifting. As a result, the $IMR^{(ph)}$ coefficient increases.

From Figs. 5 and 6, one can see that photoinduced currents do not depend on the sign of the light helicity. Taking into account the developed theoretical model, the current independence on the light helicity can be explained as follows. Circularly polarized photons generate electrons with spin polarization (Fig. 8). After the time $\Delta\tau$, photoinduced electrons can fall on exchange-split levels. The probability to occupy one of the exchange-split levels depends on electron spins. The current independence on the light helicity leads us to a conclusion that the spin-relaxation time $\tau^{(sp)}$ of photoinduced electrons is much less than the time $\Delta\tau$, $\tau^{(sp)} \ll \Delta\tau$.

Completing the consideration of the photocurrent dynamics model, we note that SiO_2(Co)/GaAs heterostructures can be used as efficient fast-response magnetic sensors. The upper frequency bound f of sensors is determined by the time t_2 (Fig. 4). From Fig. 6, one can evaluate this frequency, $f = 1/t_2 = 1$–5 MHz. If we use linear segments of current–magnetic field dependencies without hysteresis [for example, the current dependence at the voltage 70 V in the range of 150–1000 Oe in Fig. 1(b)], then high values of the current controlled by the alternating magnetic field $H(t)$,

$$j(t) = j_0 - \varsigma j_0 H(t) \tag{10}$$

can be achieved. In relation (10), j_0 is the direct current, $\varsigma j_0 H(t)$ is the alternating current, and

$$\varsigma = \frac{-1}{j_0}\frac{\partial j}{\partial H}$$

is the coefficient of the sensitivity. For the current dependence presented in Fig. 1(b) at the voltage 70 V and at the applied magnetic field H_0 in the range of 150–1000 Oe, the sensitivity coefficient ς is equal to 0.66×10^{-3} Oe^{-1}. In this case, we obtain the highest sensitivity for the alternating magnetic field $H(t)$ and reach the linearity of the sensor.

In comparison with GMR sensors, for magnetic sensors based on the IMR effect, one can attain better characteristics. The disadvantages of GMR sensors are their nonlinearity (2% for commercial devices AA002 manufactured by NVE) and hysteresis, which can reduce measurement accuracy [5,6,41–43]. The highest applicable frequency of GMR current sensors is usually lower than megahertz. In contrast to GMR sensors, for IMR sensors we can use operating conditions without hysteresis [Fig. 1(b)]. Moreover, the magnetoresistance and the linear range (850 Oe for IMR sensors versus 10.5 Oe for GMR commercial devices AA002 manufactured by NVE) are higher.

VI. CONCLUSION

We have studied relaxation processes of the light-induced giant injection magnetoresistance (IMR) in SiO_2(Co)/GaAs heterostructures, where the SiO_2(Co) structure is the granular SiO_2 film with Co nanoparticles, and have obtained the following results.

(1) Relaxation processes of the photocurrent in SiO_2(Co)/GaAs heterostructures induced by femtosecond light impulses are accompanied by relaxation oscillations. This phenomenon can be explained by the photocurrent dynamics model with exchange-split levels in the interface quantum well. Relaxation oscillations are caused by transitions between the photocurrent and electrons on the highest level in the well.

(2) The light-induced magnetoresistance $IMR^{(ph)}$ reaches the maximum value in the avalanche onset region and has

the local minimum at the higher voltage. The local minimum of the $IMR^{(ph)}$ dependence is caused by delocalization of the highest level in the interface quantum well and by decrease of the probability of the backscattering process of injected electrons on deeper levels.

(3) SiO_2(Co)/GaAs heterostructures can be used as efficient fast-response magnetic sensors operating without hysteresis at room temperature. The upper frequency bound of the sensors is of 1–5 MHz.

ACKNOWLEDGMENT

This work was supported by the Russian Science Foundation (Project No. 17-12-01314).

[1] S. A. Wolf, D. D. Awschalom, R. A. Buhrman, J. M. Daughton, S. von Molnar, M. L. Roukes, A. Y. Chtchelkanova, and D. M. Treger, Science **294**, 1488 (2001).
[2] G. Schmidt, J. Phys. D: Appl. Phys. **38**, R107 (2005).
[3] I. Žutić, J. Fabian, and S. Das Sarma, Rev. Mod. Phys. **76**, 323 (2004).
[4] J. Lenz and A. S. Edelstein, IEEE Sens. J. **6**, 631 (2006).
[5] P. Ripka and A. Tipek, *Modern Sensors Handbook* (Wiley, London, 2007).
[6] *Magnetic Sensors - Principles and Applications*, edited by K. Kuang (InTech, 2012), www.intechopen.com.
[7] L. V. Lutsev, A. I. Stognij, and N. N. Novitskii, JETP Lett. **81**, 514 (2005).
[8] L. V. Lutsev, A. I. Stognij, N. N. Novitskii, and A. A. Stashkevich, J. Magn. Magn. Mater. **300**, e12 (2006).
[9] L. V. Lutsev, A. I. Stognij, and N. N. Novitskii, Phys. Rev. B **80**, 184423 (2009).
[10] L. Lutsev, Giant injection magnetoresistance in ferromagnet/semiconductor heterostructures, in *Magnetoresistance: Types, Roles and Research*, edited by R. Gonzalez (Nova Science, New York, 2017), p. 65.
[11] M. N. Baibich, J. M. Broto, A. Fert, F. Nguyen Van Dau, F. Petroff, P. Etienne, G. Creuzet, A. Friederich, and J. Chazelas, Phys. Rev. Lett. **61**, 2472 (1988).
[12] G. Binasch, P. Grunberg, F. Saurenbach, and W. Zinn, Phys. Rev. B **39**, 4828 (1989).
[13] J. Bass and W. P. Pratt, Jr., J. Magn. Magn. Mater. **200**, 274 (1999).
[14] M. A. M. Gijs and G. E. W. Bauer, Adv. Phys. **46**, 285 (1997).
[15] X. Jiang, R. Wang, R. M. Shelby, R. M. Macfarlane, S. R. Bank, J. S. Harris, and S. S. P. Parkin, Phys. Rev. Lett. **94**, 056601 (2005).
[16] E. Y. Tsymbal, O. N. Mryasov, and P. R. LeClair, J. Phys.: Condens. Matter **15**, R109 (2003).
[17] S. S. P. Parkin, C. Kaiser, A. Panchula, P. M. Rice, B. Hughes, M. Samant, and S.-H. Yang, Nat. Mater. **3**, 862 (2004).
[18] S. Yuasa, T. Nagahama, A. Fukushima, Y. Suzuki, and K. Ando, Nat. Mater. **3**, 868 (2004).
[19] S. Yuasa, A. Fukushima, H. Kubota, Y. Suzuki, and K. Ando, Appl. Phys. Lett **89**, 042505 (2006).
[20] C. Tiusan, F. Greullet, M. Hehn, F. Montaigne, S. Andrieu, and A. Schuhl, J. Phys.: Condens. Matter **19**, 165201 (2007).
[21] Y. M. Lee, J. Hayakawa, S. Ikeda, F. Matsukura, and H. Ohno, Appl. Phys. Lett **90**, 212507 (2007).
[22] L. V. Lutsev, J. Phys.: Condens. Matter **18**, 5881 (2006).
[23] L. V. Lutsev, V. V. Pavlov, P. A. Usachev, A. A. Astretsov, A. I. Stognij, and N. N. Novitskii, Appl. Phys. Lett. **101**, 242104 (2012).
[24] V. V. Pavlov, L. V. Lutsev, P. A. Usachev, A. A. Astretsov, A. I. Stognij, N. N. Novitskii, and R. V. Pisarev, Appl. Phys. Lett. **106**, 152404 (2015).
[25] V. V. Pavlov, L. V. Lutsev, P. A. Usachev, A. A. Astretsov, A. I. Stognij, N. N. Novitskii, and R. V. Pisarev, J. Magn. Magn. Mater. **400**, 290 (2016).
[26] J. Nordling, R. L. Millen, H. A. Bullen, M. D. Porter, M. Tondra, and M. C. Granger, Anal. Chem. **80**, 7930 (2008).
[27] R. L. Millen, J. Nordling, H. A. Bullen, M. D. Porter, M. Tondra, and M. C. Granger, Anal. Chem. **80**, 7940 (2008).
[28] A. I. Stognij, N. N. Novitskii, and O. M. Stukalov, Tech. Phys. Lett. **28**, 17 (2002).
[29] T. K. Zvonareva, V. M. Lebedev, T. A. Polanskaya, L. V. Sharonova, and V. I. Ivanov-Omskii, Semiconductors **34**, 1094 (2000).
[30] E. A. Dyadkina, N. A. Grigoryeva, A. A. Vorobiev, S. V. Grigoriev, L. V. Lutsev, K. Zhernenkov, M. Wolff, D. Lott, A. I. Stognij, N. N. Novitskii, and B. P. Toperverg, Physica B **404**, 2547 (2009).
[31] N. A. Grigor'eva, A. A. Vorob'ev, V. A. Ukleev, E. A. Dyad'kina, L. V. Lutsev, A. I. Stognij, N. N. Novitskii, and S. V. Grigor'ev, JETP Lett. **92**, 767 (2010).
[32] V. A. Ukleev, N. A. Grigoryeva, E. A. Dyadkina, A. A. Vorobiev, D. Lott, L. V. Lutsev, A. I. Stognij, N. N. Novitskiy, A. A. Mistonov, D. Menzel, and S. V. Grigoriev, Phys. Rev. B **86**, 134424 (2012).
[33] M. Khodzitskiy, L. Lutsev, S. Tarapov, A. Zamkovoj, A. Stognij, and N. Novitskii, J. Magn. Magn. Mater. **320**, L37 (2008).
[34] M. K. Khodzitskiy, T. V. Bagmut, I. G. Shipkova, L. V. Lutsev, S. I. Tarapov, A. I. Stognij, and N. N. Novitskii, Telecommun. Radio Eng. **68**, 607 (2009).
[35] A. A. Stashkevich, Y. Roussigne, P. Djemia, D. Billet, A. I. Stognij, N. N. Novitskii, G. A. Wurtz, A. V. Zayats, G. Viau, G. Chaboussant, F. Ott, S. Gautrot, M. P. Kostylev, L. V. Lutsev, and V. Belotelov, J. Appl. Phys. **104**, 093912 (2008).
[36] A. A. Stashkevich, Y. Roussigne, A. I. Stognij, N. N. Novitskii, M. P. Kostylev, G. A. Wurtz, A. V. Zayats, and L. V. Lutsev, Phys. Rev. B **78**, 212404 (2008).
[37] A. A. Stashkevich, Y. Roussigne, A. I. Stognij, N. I. Novitskii, G. Wurtz, A. V. Zayats, G. Viau, G. Chaboussant, F. Ott, L. V. Lutsev, P. Djemia, M. P. Kostylev,

and V. Belotelov, J. Magn. Magn. Mater. **321**, 876 (2009).
[38] L. V. Lutsev, Phys. Solid State **44**, 102 (2002).
[39] L. V. Lutsev, Phys. Solid State **53**, 1078 (2011).
[40] V. I. Arnol'd, *Ordinary Differential Equations* (Springer-Verlag, Berlin, 1992).
[41] P. Ripka, *Magnetic Sensors and Magnetometers* (Artech House, London, 2001).
[42] *NVE Magnetic Sensor Catalog* (NVE Corporation, Eden Prairie, MN, 2012).
[43] J. Han, J. Hu, Y. Ouyang, S. X. Wang, and J. He, IEEE Trans. Ind. Electron. **62**, 516 (2015).